MICROSTRUCTURE AND HARDNESS OF ELECTRON BEAM MELTED TI-6AL-4V TITANIUM ALLOY IN DEPENDENCE OF THE SCANNING SPEED

[1]Fabrizio Coticelli and [2]Umberto Prisco

[1] *Department of Chemical, Materials and Production Engineering, University of Napoli Federiço II, Piazzale Tecchio 80, Napoli, 80125, Italy;* [2] *Department of Chemical, Materials and Production Engineering, University of Napoli Federico II, Piazzale Tecchio 80, Napoli, 80125, Italy*

Email:
{[1]umberto.prisco@uina.it,[2]fabrizio.coticelli@gmail.it}

Abstract

The effect of the beam scan velocity upon microstructure and hardness of Ti-6Al-4V titanium alloy produced by means of Electron Beam Melting (EBM) was investigated in this work. Five levels of scan velocity were used during the experimental campaign, ranging from 121 to 697 mm/s, and keeping all other process parameters fixed. It was found that a finer microstructure is generated with the increase of the beam speed, since the characteristic dimensions of both the prior columnar β grains and of the α laths decrease for higher beam speeds. In particular the finer microstructure was observed at a scan speed of 697 mm/s while the coarser at 121 mm/s. On the other side, the hardness of the EBMed samples increase with the increase of the scanning speed and a maximum hardness of about 400 HV was measured at a scan speed of 697 mm/s. This value is strictly associated to the finer microstructure that was obtained at this value of the scan speed. In particular, it was observed a 17% increase of the hardness going from a scan speed of 121 to one of 697 mm/s.

Key Words - Electron beam melting, scanning speed, microstructure, martensite, hardness.

1. Introduction

Electron Beam Melting (EBM) is a 3D printing technology for metal parts [1]. It is a manufacturing process that, depositing layer-by-layer the material, produces near-net-shape metallic components melting a metal powder by an electron beam. By being able to create mechanical parts without limits of shape EBM allows to revolutionize the approach to design [2]. Furthermore, because these advantages are connected to high energy efficiencies, EBM had found a great attention by the aerospace and biomedical industries. EBM-manufactured Ti-6Al-4V titanium alloy parts are very interesting for the aerospace and biomedical fields due to their resistance to fracturing, behavior under fatigue, resistance to corrosion, and biocompatibility [3-5].

The most recent researches on EBM study the characteristics of the final microstructure and the design of the process. The results have revealed that EBM shows certain restrictions from a technological viewpoint. It has been proven that the properties of the manufactured components are powerfully linked to the process parameters [6]. The process parameters control the thermal cycle to which the material is subjected during the manufacture and, consequently, the microstructure and mechanical strength of the EBMed part. Recently, the microstructural description of parts produced by EBM of Ti-6Al-4V titanium alloy has generated significant advances. The microstructure of Ti-6A1-4V titanium alloy produced by EBM is made up of a several phases such as α (hcp), β (bcc), and α' martensite [7, 8]. Prior Structures can also be found [9, 10]. The microstructure of EBM-built Ti-6A1-4V titanium alloy is strongly correlated with the process parameters. For example, Gong and Chou [11] investigated the link between beam speed and microstructure and found that higher beam speed resulted in a finer α lath microstructure. Gaytan et al. [12] reported that variations in the current and in the scan velocity influence the defect typology in Ti- 6Al-4V titanium alloy EBM-built parts. The heat input is likewise one of the most critical parameters in EBM of Ti- 6Al-4V titanium alloy. In this regard, it has been proved that the final microstructure is strongly related to the heat input. Other studies showed the importance of the heat input in

determining the cooling rate of the melt pool in EBM of Ti- 6Al-4V titanium alloy [13, 14].

Although various aspects of EBM of Ti-6Al-4V titanium alloy had been investigated, systematic studies about the influence of the beam scanning speed on the microstructure and hardness of EBMed parts are quite uncommon. The scope of this study is then to bring a better understanding of how this fundamental parameter comprehensively affects the microstructure, described in terms of characteristic dimensions, of both the top and the side surface, and the hardness of Ti- 6Al-4V titanium alloy parts produced by EBM.

2. Materials and Methods

A pre-alloyed Ti-6Al-4V titanium alloy powder (Grade 5, supplied in conformity to the ASTM B348 standard) was the feedstock material used to produce the samples. The powder has a particle size between 45 μm and 100 μm. Cubic specimens of 20 mm side for microstructural analysis were fabricated with an Arcam® A2 EBM system, Fig. 1. The EBM process was carried out with a constant gun-accelerating voltage of 60 kV. The thickness of the powder layer was set to 100 μm while the preheating temperature was of 730 °C. The preheating of each layer was carried out using a beam of 30 mA with a scan velocity of 15 m/s, a raster pattern of 10 passes, and a nominal vacuum of the build chamber of 10−4 torr. The deposition was carried out under a controlled vacuum of 10−2 torr reached by backfilling with helium.

To study the effect of the scan velocity upon the microstructure of the EBM-manufactured parts, various samples were fabricated with the following scan velocities: 121, 258, 409, 546, and 697 mm/s. The focus offset was 5 mA while the line offset was 0.09 mm. It must be noted that, under the chosen experimental conditions, the heat input rate (J/mm) diminishes with the increase of the scan velocity.

Ten specimens were produced for each scan velocity; consequently all data plotted in the followings must be read as the average of the 10 experiments. The measured outputs are the prior columnar β size, the prior equiaxed β size, the α lath thickness, the micro-hardness, and the weld pool dimensions. Standard metallographic techniques were used for the microstructural observations. The specimens were sectioned, mounted in resin, ground with SiC papers up to the grit size of 1200, and then lapped using diamond suspension down to 0.05 μm. The microstructure was analyzed observing different cross-sections of samples. In particular, the scanning surface, herein denoted as Z-plane, and the build side surface, herein denoted as X-plane, were examined. The polished specimens were then etched with a hydrofluoric acid-based solution (1 ml hydrofluoric acid, 50 wt.%, and 3 ml nitric acid, 60 wt.%, in 7 ml of distilled water). The

etched samples were analyzed using both an optical microscope and a scanning electron microscope (SEM). The section of the sample perpendicular to the built axis was taken at the middle plane of the specimen, corresponding to an height of 10 mm from the built plate. Microstructure evaluations were performed applying classical measurements methods commonly used in the relevant literature. To measure the hardness of the specimens, Vickers indentation tests were performed with a test load of 0.5 kgf and a loading time of 20 s.

3. Results and Discussion

Cross-sections from the X-plane of samples manufactured under the maximum, medium and minimum scan velocity respectively are shown in Fig. 1. The samples show the layered microstructure which is the characteristic fingerprint of additive processes based on powder bed fusion. The traces of the melt pools produced by the electron beam during the raster scanning are clearly identifiable and the resulting fish-scale pattern is well known in the literature on EBM [13]. As it can be observed in Fig. 1, there is an inverse correlation between the average size of the melt pool and the scan velocity.

The adding up of material layer-by-layer is associated with an iterated thermal cycle which plays as an in-situ heat treatment of annealing and homogenization for the previously deposited layers. The strength of this treatment increases with the heat input, i.e. in this case with the decrease of the scan velocity. A more intense homogenization of the microstructure during the process was obtained increasing the heat input rate with the result that the melt pool boundaries lose contrast.

The higher magnification image of Fig. 2(a) shows the typical microstructure observed on cross sections sliced along the building direction (X-plane) of the specimens [13, 14]. Columnar grains of the prior β phase are clearly identifiable. It is known that the cooling of melt pools obtained during the EBM of Ti-6Al-4V titanium alloy proceeds according to the following sequence: liquid to primary β solid phase and then $\beta \rightarrow \alpha$ or $\beta \rightarrow \alpha$ ' depending on the cooling rate, with a faster cooling inducing the formation of martensite. Previous studies [15] show that martensite transformation in Ti-6Al-4V titanium alloy from the β phase is induced for cooling rates higher than 410 °C/s. The martensite start temperature (Ms) of Ti-6Al-4V titanium alloy varies between 570 and 650 °C in function of the thermo-mechanical processing route followed during the production of the alloy [16-18].

Prior β grains nucleate and grow during the initial stage of the solidification when the temperature is higher than the β-transus temperature (~980 °C). In processes characterized by high energy transfer, like EBM, SLM, or laser cladding, the grains growing from the melt tend to

be aligned along the heat flow direction. Due to the fact that the heat flows from the melt pool to the solidified layers, i.e along the building direction (Z-axis), the β phase grains whose main orientation is close to this direction grows very fast and overruns in size less-favorably oriented neighbors [19]. The result is the formation of a columnar-shaped morphology with prior β grains grown across the built-layers of the samples.

According to previous studies [20] the nucleation of β grains occurs heterogeneously from the boundaries of the previous layers on the surface of the part under work in EBM. The texture of the prior β-grains shows that the crystals are oriented in such a way that the <001> direction points along the direction of growth. This result has been attributed to the elongated shape of the molten pool.
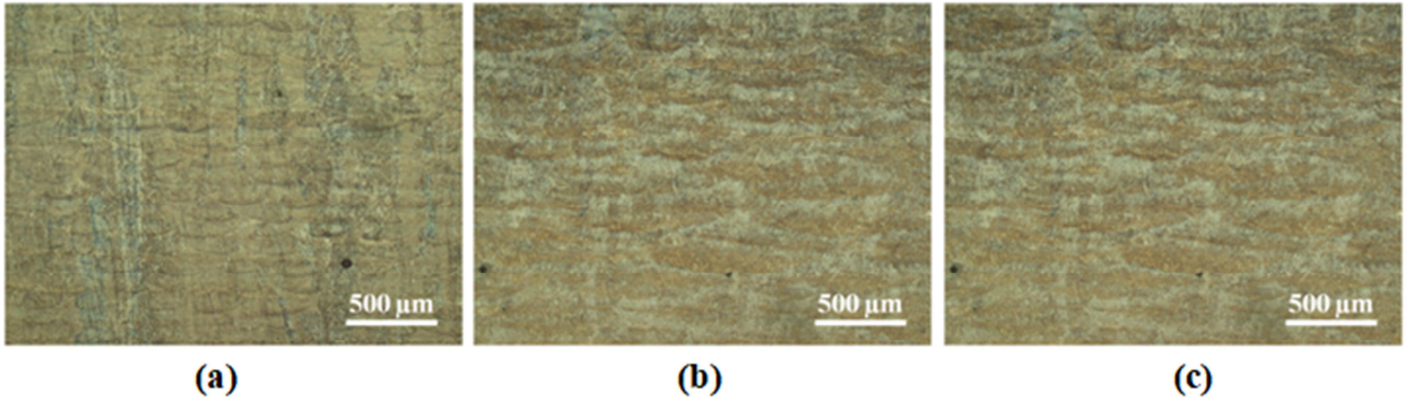

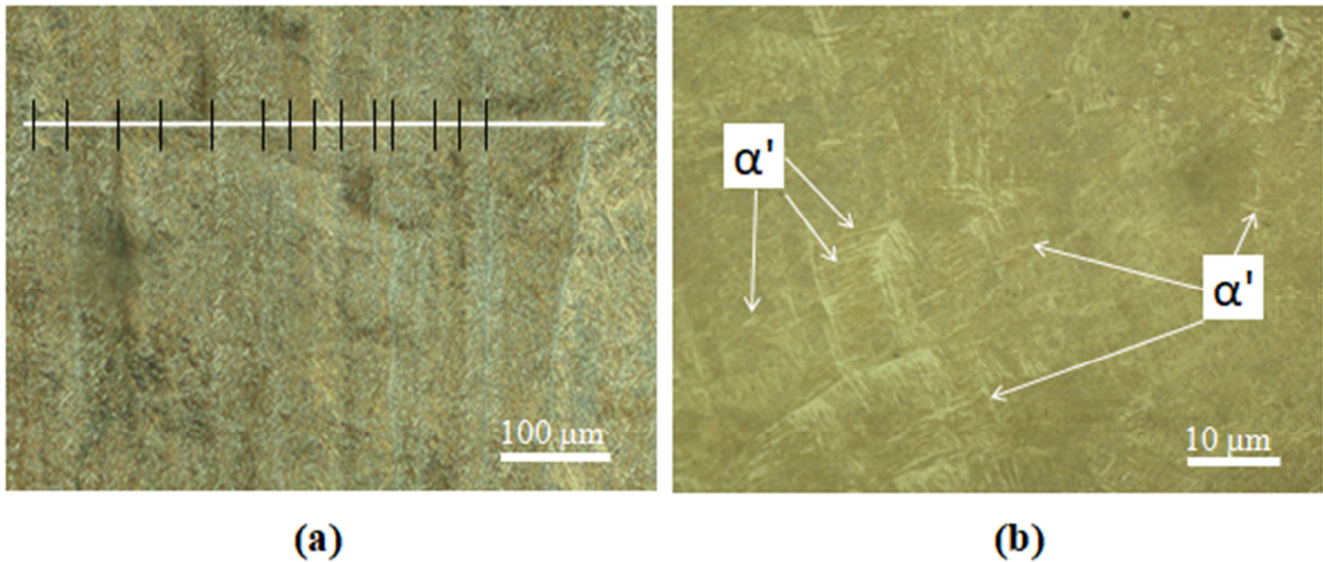Fig. 1. Macrographs of the X-plane: (a) 697 mm/s, (b) 409 mm/s, (c) 121 mm/s.

Fig. 2. Microstructure of the X-plane (side surface) from a sample processed at 546 mm/s, (a) low magnification image showing the columnar grains and width analysis, (b) high magnification image.
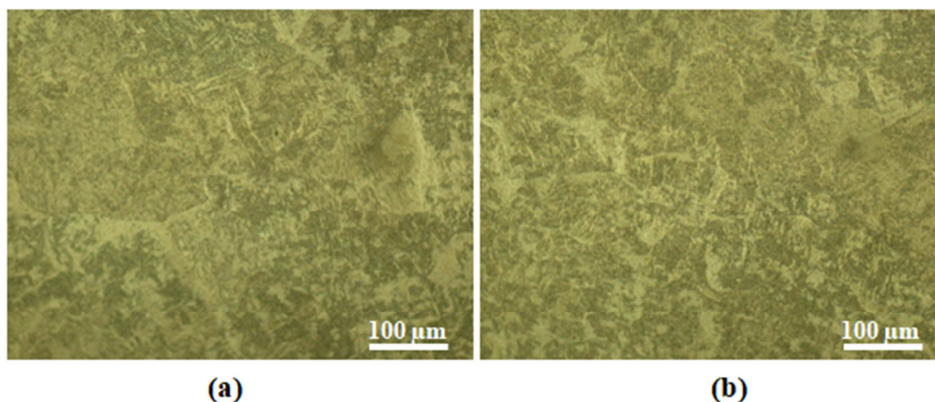
Fig. 3. Typical microstructure of the Z-plane from two EBMed samples: (a) 121 mm/s, (b) 697 mm/s.

Another typical feature of the microstructure of Ti-6Al-4V obtained by EBM is the presence of α′ martensite in the form of plates. Some α' is clearly visible within the columnar grains in the samples of Fig6. 2 (b). As already mentioned, martensite is formed from the β phase due to the high cooling rate.

The width of the prior β grains was evaluated using lines drawn normal to the columnar structure and measuring the intercepts of these lines with the boundary of the columnar grains, as shown in Fig. 2(a). Different images were examined to obtain the statistical dispersion of the measured widths. The average width of the columnar structure in Fig. 2 is 53 µm. Other authors in different conditions report values ranging from 40 to 150 µm [19].

Fig. 3 shows the typical microstructure observable on the Z-plane, namely perpendicularly to the building direction. The cross sections reported in Fig. 3 are the ones obtained from samples manufactured at the maximum and minimum scan velocity. Differently from what was observed on the transverse section, the presence of an equiaxed structure is evident. It can then be inferred that the prior β grains have a rod-like shape with the main axis oriented along the building direction. Similar microstructures were also reported by other authors [20]

All around the equiaxed crystallites, a grain boundary α (αGB) phase is visible in Fig. 4 and much more clearly in the SEM close-up of Fig. 5. This is the first α phase that nucleates from the prior β grains on cooling; this phase assumes the classical allotriomorphic morphology due to its development along the boundaries of the pre-existent structure. Additionally, fine Widmanstätten (α + β) lamellae are visible inside the prior β grains. The α laths are bordered by a small amount of β phase. This is a typical structure, also called basket-weave microstructure, in Ti-6Al-4V titanium alloy manufactured by EBM [20]. Unlike the prior β grains the α laths show no preferred orientation. The

Widmanstätten lamellae however present a finer grained structure than the corresponding microstructure of a wrought or cast Ti-6Al-4V titanium alloy. Some martensite is also visible in Fig. 5.

The mean intercept method was used to measure the dimension of the equiaxed grains and the width of the α laths.

The influence of the scan velocity is shown in Fig. 6. This figure plots the average columnar β size, the equiaxed β size, and the α lath thickness against the scan velocity.

It is quite evident from Fig. 6 that all the measured microstructural features are inversely proportional to the scan velocity. E.g. the columnar β size shrinks from 131 µm to 48 µm when the scan velocity arises from 121 mm/s to 697 mm/s. The α lath thickness decreases from 1.8 µm to 1 µm under the same conditions.
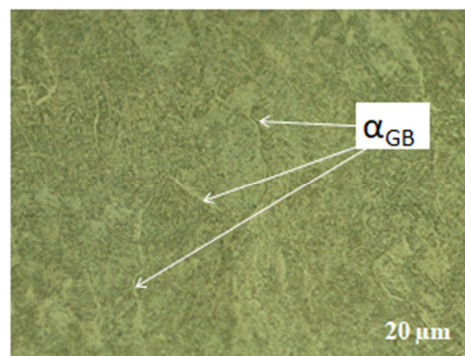

Fig. 4. Typical microstructure of the Z-plane from a sample

processed at 121 mm/s.

The trends observed in Fig. 6 can be explained by the different cooling rates resultant from the different scan velocity. Lower scan rates, which causes higher heat input rates, are coupled to lower cooling rates and thus generate a coarser microstructure of both columnar and equiaxed β

grains, see Fig. 6 (a) and (b) . Other authors have confirmed that the earlier finer β grains are produced by an increase in cooling rate. Similarly, the size of the α laths increases with the decrease of the scan velocity, i.e. with the increase of the heat input. Indeed, the transformation of Widmanstätten in Ti-6Al-4V titanium alloy is much influenced by the cooling rate; in particular, it is known that lower cooling rates favor the precipitation of larger α-laths [18].
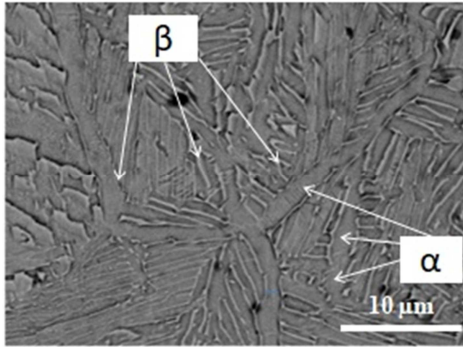

Fig. 5. SEM micrograph from the Z-plane of an EBMed

sample processed at 409 mm/s.

Higher cooling rates promote an increased formation of martensite. Indeed, larger volume fractions of α' martensite were observed in conditions of lower heat input. Due to the lack of a method to measure the amount of martensite in the samples it was not possible to quantify this relation.

The Vickers hardness of the samples is plotted in Fig. 7. The finest microstructures observed at 697 mm/s resulted in the highest microhardness. The data indicates that the hardness is inversely proportional to the microstructure coarseness. There is a drop of 60 HV along the range of measured lath thickness, from 1 µm to 1.8 µm. It is evident that the higher martensite content caused by the increase on the scan velocity influences the hardness of the sample. These results are in agreement with the well-known effect of the microstructural refinement upon the mechanical strength and are a confirmation of the above described relation between the cooling rate and the microstructure, see Fig. 6. The measured hardness is in good accordance with earlier values reported for EBM-manufactured Ti-6Al-4V titanium alloy [20].
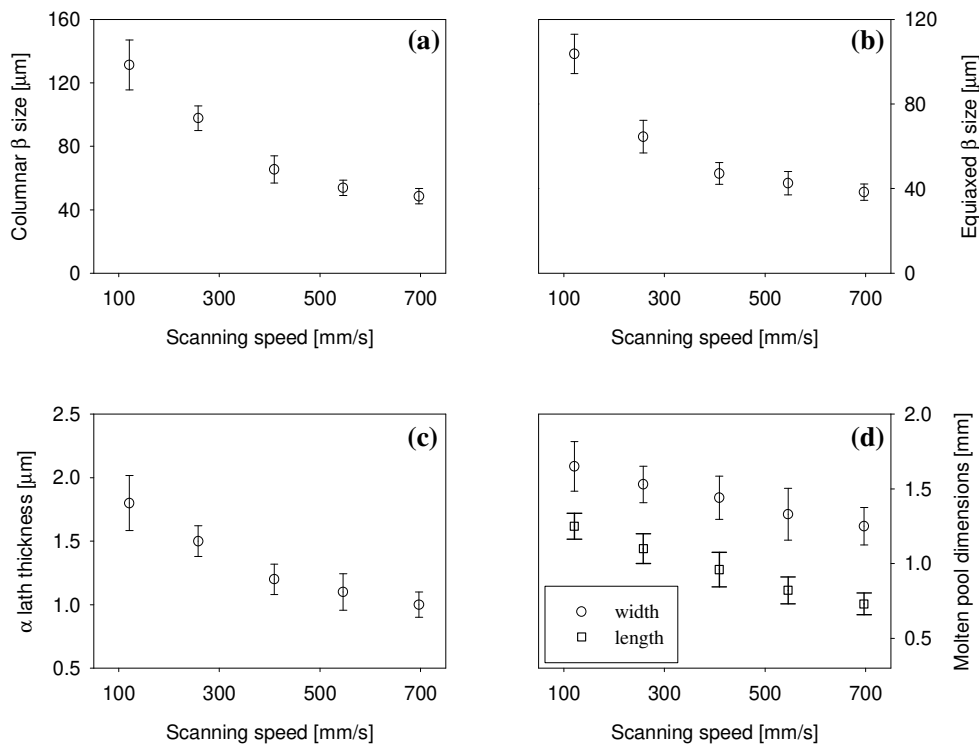

Fig. 6. (a) Columnar β size, (b) equiaxed β size, (c) α lath thickness, and (d) melt pool dimensions of the samples as function of

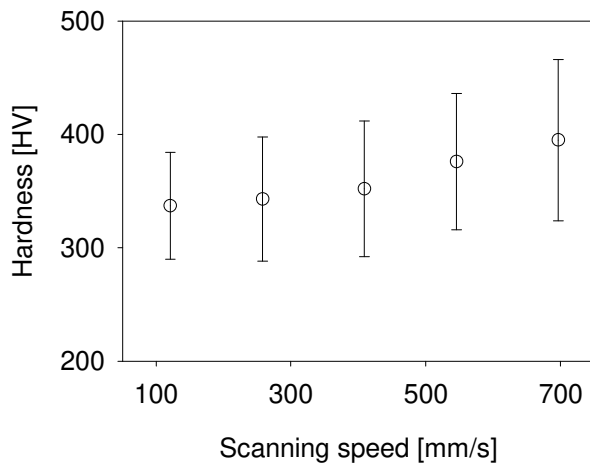the scan speed (error bars represent the 95% confidence intervals).

Fig. 7. Hardness of the samples as function of the

scanning speed (error bars represent the 95% confidence

intervals).

4.   Conclusions

The major conclusions are summarized as follows.

The X-plane (side surface) shows columnar prior β grains of width in the range 48-131 µm. The Z-plane (scanning surface) presents equiaxed grains with size varying between 38 and 103 µm. The equiaxed grains show a Widmanstätten (α + β) microstructure with α lath thickness in the range 1-1.8 µm. Martensite platelets are also visible.

There is a clear relation between the increase in the scan velocity and the increase in fineness of the microstructure. This is due to the latter being related to the cooling rate of the melt pools, cooling rate that is proportional to the scan velocity.

Future researches shall be oriented towards the optimization of the microstructure, in order to obtain EBMed parts conforming to the required properties, as well as towards the minimization of surface roughness while respecting economic and productivity constraints.

References

[1] Varun Teja P., Sivaprakash R., Vinay Krishnan V., Vasanth, Potential and scope of additive manufacturing in aerospace industry with reference to India, International Journal of Innovative Technology and Exploring Engineering, 8 (6 Special Issue 4), 2019, 1085-1089,

[2]   Venkata Ramana M., Sharma A., Krishna Mohan Rao G., Hanumantha Rao D., Chenna Kesava Rao B. Optimization of controllable process parameters to decrease cutting forces in turning of Ti6Al4V alloy with various machining environments, Journal of Manufacturing Technology Research, 11(3-4), 2019, 81-100.

[3] Prisco U. Shape of the melt pool produced by a moving Gaussian heat source, Welding in the World, 65(11), 202, 2105-2118.

[4]   Pandit A., Sekhar R., Shah P., Simulation based process optimization for additive manufacturing, International Journal of Innovative Technology and Exploring Engineering, 8 (10), 2019, 3405-3410

[5]   Zhang Y., Li Q., Guo X., Chen Y. The Sintering Densification and Microstructure Evolutions of Ti-1Al-8V-5Fe Alloy with Si Additions (2019) Materials and Manufacturing Processes, 34, 907-914.

[6]   Venkata Ramana M., Sharma A., Krishna Mohan Rao G., Hanumantha Rao D., Chenna Kesava Rao B. Optimization of controllable process parameters to decrease cutting forces in turning of Ti6Al4V alloy with various machining environments, Journal of Manufacturing Technology Research, 11(3-4), 2019, 81-100.

[7]   Thesiya D., Rajurkar A., Patel S. Heat affected zone and recast layer of ti-6al-4v alloy in the EDM process through scanning electron microscopy (SEM) (2014) Journal of Manufacturing Technology Research, 6(1-2), pp. 41-47.

[8]   Bingham B.C., Parmigiani J.P. The use of ECM capsules for the machining of inconel and titanium, Journal of Manufacturing Technology Research, 6(3-4), 2014, 83-91.

[9]   Tiwary A.P., Pradhan B.B., Bhattacharyya B. Parametric optimization of micro-EDM process using response surface methodology and principal component analysis, Journal of Manufacturing Technology Research, 5(3-4), 2014, 117-136.

[10] Negi S., Dhiman S., Sharma R.K. Basics, applications and future of additive manufacturing technologies: A review, Journal of Manufacturing Technology Research, 5(1-2), 2013, 75-96.

[11] Gong X., Lydon J., Cooper K., Chou K. Beam Speed Effects on Ti–6Al–4V Microstructures in Electron Beam Additive Manufacturing, Journal of Materials Research, 29, 2014, 1951-1959.

[12] Gaytan S.M., Murr L.E., Medina F., Martinez E., Lopez M.I., Wicker R.B. Advanced Metal Powder Based Manufacturing of Complex Components by Electron Beam Melting, Materials Technology, 24, 2009, 180-190.

[13]   Singh S., Sachdeva A., Sharma V.S. A study on selective laser sintered parts for dimensional and surface characteristics, Journal of Manufacturing Technology Research, 4(3-4), 2012, 145-157.

[14]   Al-Bermani S.S. An Investigation into Microstructure and Microstructural Control of Additive Layer Manufactured Ti-6Al-4V by Electron Beam Melting. University of Sheffield, 2011.

[15]   François M., Han S., Segonds F., Dupuy C., Rivette M., Turpault S., Mimouna M., Salvatore F., Rech, J., Peyre, P. Electromagnetic performance of Ti6Al4V and AlSi7Mg0.6 waveguides with laser beam melting (LBM) produced and abrasive flow machining (AFM) finished internal surfaces, Journal of Electromagnetic Waves and Applications, 35(18), 2021, 2510-2526.

[16]   Kalaiselvan K., Elango A., Nagarajan N.M. Age hardening treatment on Ti/Al dissimilar metal laser beam welded joint to suppress distortion, Journal of Manufacturing Technology Research, 7(1-2), 2015, 89-99 .

[17]   Kalaiselvan K., Elango A., Nagarajan N.M. Crack and surface morphology on dissimilar metal butt joints using laser beam welding, Journal of Manufacturing Technology Research, 7(3-4), 2015, 129-139.

[18]   Chen J., Chen X., Liu X., Wei Y. Numerical investigation on keyhole stability and weld pool dynamics during quasi-continuous

laser beam welding of Ti6Al4V plate using constant and modulated high-frequency pulsed heat input, International Journal of Advanced Manufacturing Technology, 121(1-2), 2022, 229-247.

[19]   Gong X., Lydon J., Cooper K., Chou K. Beam speed effects on Ti-6Al-4V microstructures in electron beam additive manufacturing, Journal of Materials Research, 29(17), 2014, 1951-1959.

[20]   Alsaddah M., Khan A., Groom K., Mumtaz K. Diode area melting of Ti6Al4V using 808 nm laser sources and variable multi-beam profiles, Materials and Design, 215, 2022, 110518.